

Demodulation of a positron beam in a bent crystal channel

A. Kostyuk^a, A.V. Korol^{a,b}, A.V. Solov'yov^a, Walter Greiner^a

^a*Frankfurt Institute for Advanced Studies, Johann Wolfgang Goethe-Universität,
Ruth-Moufang-Str. 1, 60438 Frankfurt am Main, Germany*

^b*Department of Physics, St Petersburg State Maritime Technical University, St
Petersburg, Russia*

Abstract

The evolution of a modulated positron beam in a planar crystal channel is investigated within the diffusion approach. A detailed description of the formalism is given. A new parameter, the demodulation length, is introduced, representing the quantitative measure of the depth at which the channelling beam preserves its modulation in the crystal. It is demonstrated that there exist crystal channels with the demodulation length sufficiently large for using the crystalline undulator as a coherent source of hard X rays. This finding is a crucial milestone in developing a new type of lasers radiating in the hard X ray and gamma ray range.

Keywords:

PACS: 61.85.+p, 05.20.Dd, 41.60.-m

1. Introduction

In this article we study the evolution of a modulated positron beam in straight and bent planar crystal channels. Some key ideas of this research were briefly communicated in [1] and [2]. In this paper we present a systematic and detailed description of the formalism and the obtained results. The outcome of the research is of crucial importance for the theory of the crystal

Email addresses: kostyuk@fias.uni-frankfurt.de (A. Kostyuk),
a.korol@fias.uni-frankfurt.de (A.V. Korol), solovyov@fias.uni-frankfurt.de
(A.V. Solov'yov)

undulator based laser (CUL) [3, 4, 5] — a new electromagnetic radiation source in hard x- and gamma-ray range.

Channelling takes place if charged particles enter a single crystal at small angle with respect to crystallographic planes or axes [6]. The particles get confined by the interplanar or axial potential and follow the shape of the corresponding planes and axes. This suggested the idea [7] of using bent crystals to steer the particles beams. Since its first experimental verification [8] the idea to deflect or extract high-energy charged particle beams by means of tiny bent crystals replacing huge dipole magnets has been attracting a lot of interest worldwide. Bent crystal have been routinely used for beam extraction in the Institute for High Energy Physics, Russia [9]. A series of experiments on the bent crystal deflection of proton and heavy ion beams was performed at different accelerators [10, 11, 12, 13, 14] throughout the world. The bent crystal method has been proposed to extract particles from the beam halo at CERN Large Hadron Collider [15] The possibility of deflecting positron [16] and electron [14, 17] beams has been studied as well.

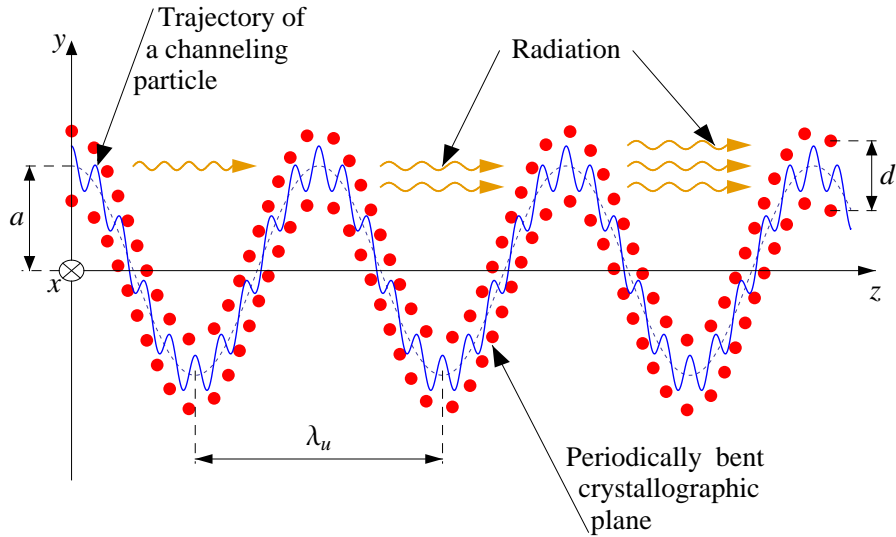


Figure 1: Schematic representation of the crystalline undulator.

A single crystal with *periodically* bent crystallographic planes can force channelling particles to move along nearly sinusoidal trajectories and radiate in the hard x- and gamma-ray frequency range (see figure 1). The feasibility

of such a device, known as the 'crystalline undulator', was demonstrated theoretically a decade ago [3] (further developments as well as historical references are reviewed in [18]). More recently, an electron based crystalline undulator has been proposed [19].

It was initially suggested to obtain sinusoidal bending by the propagation of an acoustic wave along the crystal [3, 4]. The advantage of this approach is its flexibility: the period of deformation can be chosen by tuning the frequency of the ultrasound. However, this approach is rather challenging technologically and yet to be tested experimentally. Several other technologies for the manufacturing of periodically bent crystals have been developed and tested. These include making regularly spaced grooves on the crystal surface either by a diamond blade [20, 21] or by means of laser-ablation [22], deposition of periodic Si_3N_4 layers onto the surface of a Si crystal [21], growing of $\text{Si}_{1-x}\text{Ge}_x$ crystals [23] with a periodically varying Ge content x [24, 25].

Experimental studies of the crystalline undulator are currently in progress. The first results are reported in [26] and [27].

The advantage of the crystalline undulator is in extremely strong electrostatic fields inside a crystal which are able to steer the particles much more effectively than even the most advanced superconductive magnets. This fact allows to make the period λ_u of the crystalline undulator in the range of hundreds or tens micron which is two to three orders of magnitude smaller than that of conventional undulator. Therefore the wavelength of the produced radiation $\lambda \sim \lambda_u/(2\gamma^2)$ ($\gamma \sim 10^3$ – 10^4 being the Lorentz factor of the particle) can reach the (sub)picometer range, where conventional sources with comparable intensity are unavailable [28].

Even more powerful and coherent radiation will be emitted if the probability density of the particles in the beam is modulated in the longitudinal direction with the period λ , equal to the wavelength of the emitted radiation (see figure 2). In this case, the electromagnetic waves emitted in the forward direction by different particles have approximately the same phase [29]. Therefore, the intensity of the radiation becomes proportional to the beam density squared (in contrast to the linear proportionality for an unmodulated beam). This increases the photon flux *by orders of magnitude* relative to the radiation of unmodulated beam of the same density. The radiation of a modulated beam in an undulator is a keystone of the physics of free-electron lasers (FEL) [30, 31]. It can be considered as a classical counterpart of the stimulated emission in quantum physics. Therefore, if similar phenomenon takes place in a crystalline undulator, it can be referred to as

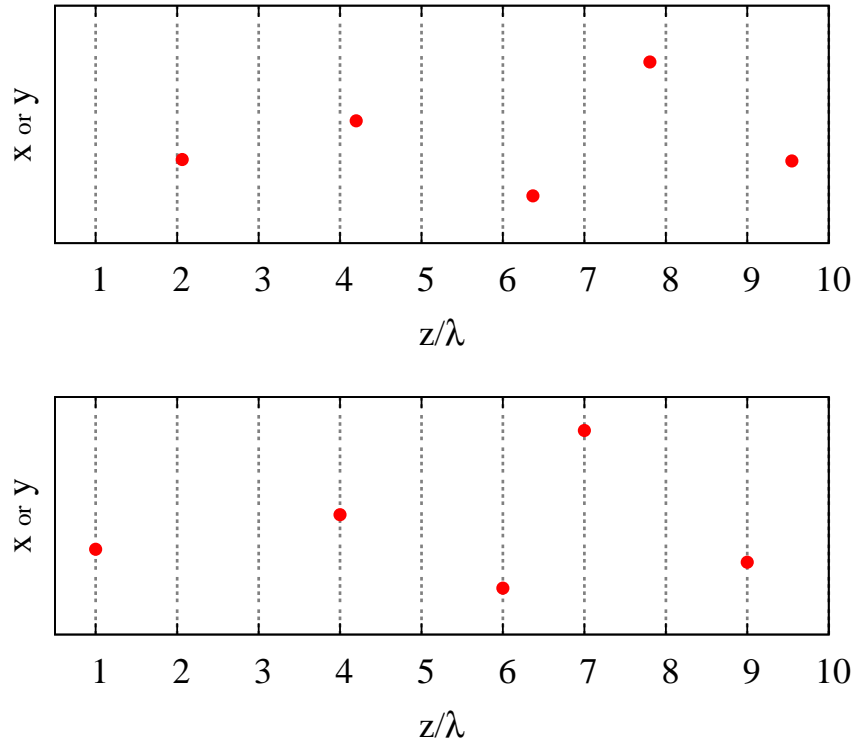


Figure 2: In an unmodulated beam (the upper panel) the particles are randomly distributed. In a completely modulated beam (the lower panel) the distance between any two particles along the beam direction is an integer multiple of the modulation period λ .

the *lasing regime of the crystalline undulator*.

The feasibility of CUL radiating in the hard x-ray and gamma-ray range was considered for the first time in [3, 4]. Recently, a two-crystal scheme, the gamma klystron, has been proposed [5].

A simplified model used in the cited papers assumed that all particle trajectories follow exactly the shape of the bent channel. In reality, however, the particle moving along the channel also oscillates in the transverse direction with respect to the channel axis (see the shape of the trajectory in figure 1). Different particles have different amplitudes of the oscillations inside the channel (figure 3, upper panel). Similarly, the directions of particle momenta in (xz) plane are slightly different (figure 3, lower panel). Even if the speed of the particles along their trajectories is the same, the particles oscillat-

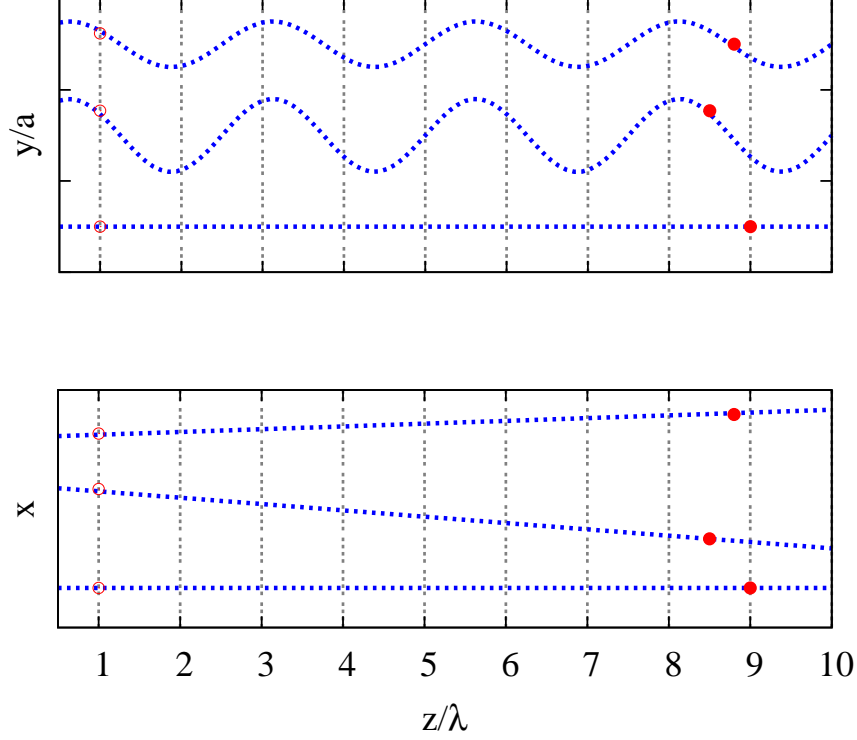


Figure 3: Due to different amplitudes of channelling oscillation (upper panel) and different momentum directions in the (xz) plane (lower panel), the initially modulated beam gets demodulated. The open and filled circles denote the same particles at the crystal entrance and after travelling some distance in the crystal channel, respectively.

ing with different amplitudes or the particles with different trajectory slopes with respect to z axis have slightly different components of their velocities along the channel. As a result, the beam gets demodulated. An additional contribution to the beam demodulation comes from incoherent collisions of the channelling particles with the crystal constituents.

In the case of an unmodulated beam, the length of the crystalline undulator and, consequently, the maximum accessible intensity of the radiation are limited by the dechannelling process. The channelling particle gradually gains the energy of transverse oscillation due to collisions with crystal constituents. At some point this energy exceeds the maximum value of the interplanar potential and the particle leaves the channel. The average pen-

etration length at which this happens is known as the *dechannelling length*. The dechannelled particle no longer follows the sinusoidal shape of the channel and, therefore, does not contribute to the undulator radiation. Hence, the reasonable length of the crystalline undulator is limited to a few dechannelling lengths. A longer crystal would attenuate rather than produce the radiation. Since the intensity of the undulator radiation is proportional to the undulator length squared, the dechannelling length and the attenuation length are the main restricting factors that have to be taken into account when the radiation output is calculated.

In contrast, not only the shape of the trajectory but also the particles positions with respect to each other along z axis are important for the lasing regime. If these positions become random because of the beam demodulation, the intensity of the radiation drops even if the particles are still in the channelling mode. Hence, it is the beam demodulation rather than dechannelling that restricts the intensity of the radiation of CUL. Understanding this process and estimating the characteristic length at which this phenomenon takes place is, therefore, a cornerstone of the theory of this new radiation source.

2. Diffusion Equation

2.1. The model of the crystal channel

We adopt the following model of the planar crystal channel (see Fig. 2.1):

- the interplanar potential is approximated with a parabola

$$U(\rho) = U_{\max} \left(\frac{\rho}{\rho_{\max}} \right)^2 \quad (1)$$

(ρ is the distance from the potential minimum) so that the channeling oscillations are assumed to be harmonic;

- the electron density within the distance of one Thomas-Fermi radius of the crystal atoms from the crystallographic plane is assumed to be so high that the particle gets quickly scattered out of the channel. Therefore, the particle is considered dechanneled just after it enters this region. So that the effective channel width is $2\rho_{\max} = d - 2a_{\text{TF}}$, where d and a_{TF} are respectively the interplanar distance and is the Thomas-Fermi radius.

As is seen from the figure, the parabolic approximation is quite reasonable. The real potential differs from the parabola mostly in the region of high electron density, where the particle assumes to be dechanneled.

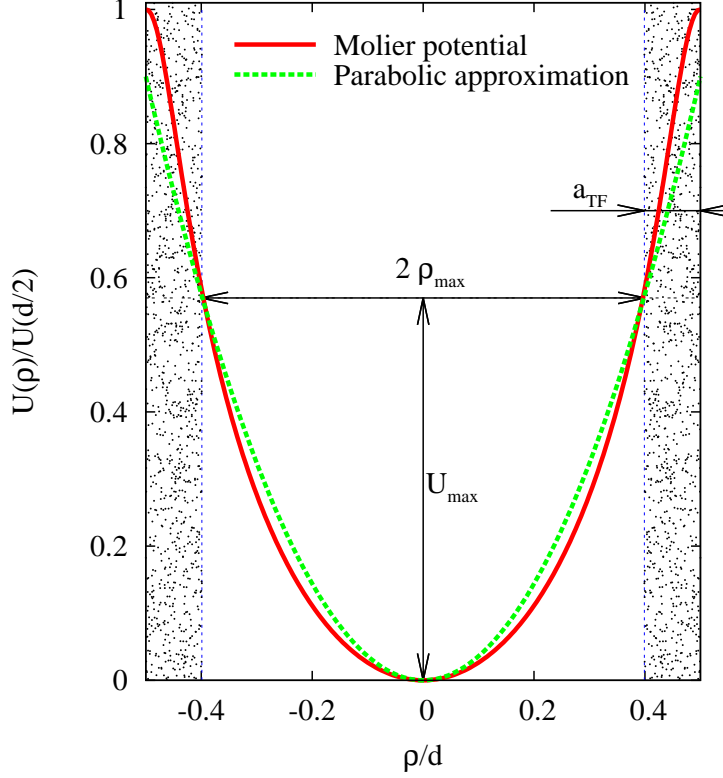


Figure 4: The model of the plane crystal channel. The interplanar potential is approximated by a parabola. It is assumed that the particle dechannels if it enters the vicinity of the crystallographic plane within the Thomas-Fermi radius, a_{TF} .

2.2. The particle distribution

Let us consider the distribution $f(t, s; \xi, E_y)$ of the beam particles with respect to the angle between the particle trajectory and axis z in the (xz) plane $\xi = \arcsin p_x/p \approx p_x/p$ and the energy of the channeling oscillation $E_y = p_y^2/2E + U(y)$ ¹. Here p , p_x and p_y are, respectively, the particle momentum and its x and y components, and E is the particle energy (we will consider only ultrarelativistic particles, therefore $E \approx p$).

¹We chose the system of units in such a way that the speed of light is equal to unity. Therefore, mass, energy and momentum have the same dimensionality. This is also true for length and time.

2.3. Kinetic equation

In absence of random scattering, the distribution function $f(t, z; \xi, E_y)$ would satisfy the differential equation $\frac{\partial f}{\partial t} + \frac{\partial f}{\partial z} v_z = 0$, where $v_z \equiv \frac{\partial z}{\partial t}$. In reality, however, the right-hand-side of the equation is not zero. It contains the collision integral. After averaging over the period of the channeling oscillation, the kinetic equation takes the form

$$\frac{\partial f}{\partial t} + \frac{\partial f}{\partial z} \langle v_z \rangle = \left\langle \iint d\xi dE'_y [f(t, z; \xi', E'_y) w(\xi', E'_y; \xi, E_y) - f(t, z; \xi, E_y) w(\xi, E_y; \xi', E'_y)] \right\rangle \quad (2)$$

where $w(\xi, E_y; \xi', E'_y) dz$ is the probability that the particle changes its angle ξ and transverse energy from ξ and E_y to, respectively, ξ' and E'_y while travelling the distance dz . The angular brackets stand for averaging over the period of the channeling oscillations.

Due to the detailed equilibrium

$$w(\xi, E_y; \xi', E'_y) = w(\xi', E'_y; \xi, E_y) \quad (3)$$

2.4. Diffusion approximation

We assume that soft scattering dominates, i.e. the function $w(\xi', E'_y; \xi, E_y)$ is not negligible only if $|\xi' - \xi|$ and $|E'_y - E_y|$ are small so that $f(t, z; \xi', E'_y) \equiv f(t, z; \xi + \vartheta_x, E_y + q_y)$ can be expanded into the Taylor series with respect to ϑ_x and q_y . Then, up to the second order in ϑ_x and q_y , one obtains

$$\frac{\partial f}{\partial t} + \frac{\partial f}{\partial z} \langle v_z \rangle = D_\xi \frac{\partial f}{\partial \xi} + D_y \frac{\partial f}{\partial E_y} + D_{\xi\xi} \frac{\partial^2 f}{\partial \xi^2} + D_{\xi y} \frac{\partial^2 f}{\partial \xi \partial E_y} + D_{yy} \frac{\partial^2 f}{\partial E_y^2} \quad (4)$$

where

$$D_\xi = \left\langle \int d\vartheta_x \vartheta_x \int dq_y w(\xi, E_y; \xi + \vartheta_x, E_y + q_y) \right\rangle \quad (5)$$

$$D_y = \left\langle \int d\vartheta_x \int dq_y q_y w(\xi, E_y; \xi + \vartheta_x, E_y + q_y) \right\rangle \quad (6)$$

$$D_{\xi\xi} = \frac{1}{2} \left\langle \int d\vartheta_x \vartheta_x^2 \int dq_y w(\xi, E_y; \xi + \vartheta_x, E_y + q_y) \right\rangle \quad (7)$$

$$D_{\xi y} = \left\langle \int d\vartheta_x \vartheta_x \int dq_y q_y w(\xi, E_y; \xi + \vartheta_x, E_y + q_y) \right\rangle \quad (8)$$

$$D_{yy} = \frac{1}{2} \left\langle \int d\vartheta_x \int dq_y q_y^2 w(\xi, E_y; \xi + \vartheta_x, E_y + q_y) \right\rangle \quad (9)$$

3. Diffusion Coefficient

3.1. Scattering

Let us consider a channeling positron colliding with a target electron. If θ is the scattering angle in the lab frame and φ is the angle between the scattering plane and the (xz) -plane then the transverse components of the particle momentum are changed by

$$\delta p_x = p \sin \theta \cos \varphi, \quad (10)$$

$$\delta p_y = p \sin \theta \sin \varphi, \quad (11)$$

As far as $\theta \ll 1$, we can use the approximation $\sin \theta \approx \theta$. Then

$$\vartheta_x = \frac{p_x + \delta p_x}{p} - \frac{p_x}{p} = \frac{\delta p_x}{p} = \theta \cos \varphi. \quad (12)$$

and

$$\begin{aligned} q_y &= \left(\frac{(p_y + \delta p_y)^2}{2E} + U(y) \right) - \left(\frac{p_y^2}{2E} + U(y) \right) \\ &= p_y \theta \sin \varphi + \frac{p}{2} \theta^2 \sin^2 \varphi. \end{aligned} \quad (13)$$

3.2. The transition probability

The probability for the particle to be scattered by an electron from the state (ξ, E_y) to the state $(\xi + \vartheta_x, E_y + q_y)$ while travelling the distance dz can be related to the differential cross section of positron-electron scattering:

$$\begin{aligned} w(\xi, E_y; \xi + \vartheta_x, E_y + q_y) dz &= n_e dz \int d\theta \int_0^{2\pi} d\varphi \frac{d^2\sigma}{d\theta d\varphi} \\ &\quad \delta(\theta \cos \varphi - \vartheta_x) \delta\left(p_y \theta \sin \varphi + \frac{p}{2} \theta^2 \sin^2 \varphi - q_y\right) \end{aligned} \quad (14)$$

Because both target and projectile are not polarized, the cross section does not depend on φ :

$$\frac{d^2\sigma}{d\theta d\varphi} = \frac{1}{2\pi} \frac{d\sigma}{d\theta}. \quad (15)$$

Substituting (14) into (5)–(9) and integrating over ϑ_x and q_y one obtains

$$D_\xi = \frac{1}{2\pi} \left\langle n_e \int d\theta \int_0^{2\pi} d\varphi \frac{d\sigma}{d\theta} \theta \cos \varphi \right\rangle \quad (16)$$

$$D_y = \frac{1}{2\pi} \left\langle n_e \int d\theta \int_0^{2\pi} d\varphi \frac{d\sigma}{d\theta} \left(p_y \theta \sin \varphi + \frac{p}{2} \theta^2 \sin^2 \varphi \right) \right\rangle \quad (17)$$

$$D_{\xi\xi} = \frac{1}{4\pi} \left\langle n_e \int d\theta \int_0^{2\pi} d\varphi \frac{d\sigma}{d\theta} \theta^2 \cos^2 \varphi \right\rangle \quad (18)$$

$$D_{\xi y} = \frac{1}{2\pi} \left\langle n_e \int d\theta \frac{d\sigma}{d\theta} \int_0^{2\pi} d\varphi \theta \cos \varphi \left(p_y \theta \sin \varphi + \frac{p}{2} \theta^2 \sin^2 \varphi \right) \right\rangle \quad (19)$$

$$D_{yy} = \frac{1}{4\pi} \left\langle n_e \int d\theta \frac{d\sigma}{d\theta} \int_0^{2\pi} d\varphi \theta^2 \sin^2 \varphi \left(p_y + \frac{p}{2} \theta \sin \varphi \right)^2 \right\rangle \quad (20)$$

Then integration over φ and neglecting higher order terms with respect to θ yields

$$D_\xi = 0 \quad (21)$$

$$D_y = \frac{p}{4} \langle n_e \rangle \int d\theta \frac{d\sigma}{d\theta} \theta^2 \quad (22)$$

$$D_{\xi\xi} = \frac{1}{4} \langle n_e \rangle \int d\theta \frac{d\sigma}{d\theta} \theta^2 \quad (23)$$

$$D_{\xi y} = 0 \quad (24)$$

$$D_{yy} = \frac{1}{4} \langle n_e p_y^2 \rangle \int d\theta \frac{d\sigma}{d\theta} \theta^2 \quad (25)$$

Here $\langle n_e \rangle$ is the electron density along the particle trajectory averaged over the period of the channeling oscillations. Generally speaking, $\langle n_e \rangle$ depends on the transverse energy E_y . We assume, however, that the electron density does not change essentially within the channel. Therefore, $\langle n_e \rangle$ can be treated as a constant. For the same reason, we can make the approximation $\langle n_e p_y^2 \rangle \approx \langle n_e \rangle \langle p_y^2 \rangle$. Then $\langle p_y^2 \rangle = 2E \left\langle \frac{p_y^2}{2E} \right\rangle = EE_y$. due to the virial theorem for the harmonic potential: $p_y^2/(2E) = E_y/2$

Finally, one obtains for nonzero coefficients

$$D_y \equiv D_0 \quad (26)$$

$$D_{\xi\xi} = \frac{1}{E} D_0 \quad (27)$$

$$D_{yy} = E_y D_0 \quad (28)$$

The diffusion equation takes the form

$$\frac{\partial f}{\partial t} + \frac{\partial f}{\partial z} \langle v_z \rangle = D_0 \left[\frac{\partial}{\partial E_y} \left(E_y \frac{\partial f}{\partial E_y} \right) + \frac{1}{E} \frac{\partial^2 f}{\partial \xi^2} \right]. \quad (29)$$

Equation (29) is akin to the equation describing dechanneling process (see e.g. [32]). The novel feature of it is the presence of time variable, which allows to describe time dependent (modulated) beams. Additionally, it takes into account scattering in the (x, z) plane.

4. Solving the diffusion equation

4.1. The average longitudinal velocity

The particle velocity along z axes averaged over the period of channeling oscillations can be represented as

$$\langle v_z \rangle = \frac{\sqrt{1 - \frac{1}{\gamma^2}} \cos \xi}{\frac{k_c}{2\pi} \int_0^{2\pi/k_c} \sqrt{1 + [bk_c \sin(k_c z)]^2} dz}. \quad (30)$$

Here $\sqrt{1 - 1/\gamma^2}$ is the particle speed along the trajectory, $\cos \xi \approx (1 - \xi^2/2)$ appears because of the slope $\xi \ll 1$ of the trajectory to z axis in (xz) plane, and the denominator is due to the sinusoidal channeling oscillations in (xy) plane with the amplitude b and the period $\lambda_c = 2\pi/k_c$. Taking into account that the amplitude of the channeling oscillations is much smaller than their period, $bk_c \ll 1$, the denominator can be approximated by $1 + (bk_c)^2/4$. For the harmonic potential (1) (see Fig. 2.1) the amplitude b is related to the transverse energy E_y by

$$b = \rho_{\max} \sqrt{\frac{E_y}{U_{\max}}}. \quad (31)$$

Using the formula for the frequency of the harmonic oscillator one finds

$$k_c = \sqrt{\frac{1}{E} \frac{d^2 U}{d\rho^2}} = \frac{1}{\rho_{\max}} \sqrt{\frac{2U_{\max}}{E}} \quad (32)$$

So that $bk_c = \sqrt{\frac{2E_y}{E}}$. Finally, neglecting higher order terms

$$\langle v_z \rangle \approx \left(1 - \frac{1}{2\gamma^2} - \frac{\xi^2}{2} - \frac{E_y}{2E} \right) \quad (33)$$

4.2. Excluding the time variable

If the beam is periodically modulated (bunched) the distribution $f(t, z; \xi, E_y)$ can be represented as a Fourier series:

$$f(t, z; \xi, E_y) = \sum_{j=-\infty}^{\infty} g_j(z; \xi, E_y) \exp(ij\omega t). \quad (34)$$

with $g_j^*(z; \xi, E_y) = g_{-j}(z; \xi, E_y)$ to ensure the real value of the particle distribution. Since Eq. (29) is linear, it is sufficient to consider only one harmonic. Substituting $f(t, z; \xi, E_y) = g(z; \xi, E_y) \exp(i\omega t)$ into (29) one obtains

$$i\omega g(z; \xi, E_y) + \frac{\partial g}{\partial z} \langle v_z \rangle = D_0 \left[\frac{\partial}{\partial E_y} \left(E_y \frac{\partial g}{\partial E_y} \right) + \frac{1}{E} \frac{\partial^2 g}{\partial \xi^2} \right]. \quad (35)$$

4.3. Variable separation

To simplify this equation, we make the substitution

$$g(z; \xi, E_y) = \exp(-i\omega z) \tilde{g}(z; \xi, E_y), \quad (36)$$

where $\tilde{g}(z; \xi, E_y)$ varies slowly comparing to $\exp(-i\omega z)$:

$$\partial \tilde{g} / \partial z \ll \omega \tilde{g}(z; \xi, E_y). \quad (37)$$

Equation (35) takes the form

$$\frac{\partial \tilde{g}}{\partial z} \langle v_z \rangle + i\omega \tilde{g}(z; \xi, E_y) (1 - \langle v_z \rangle) = D_0 \left[\frac{\partial}{\partial E_y} \left(E_y \frac{\partial \tilde{g}}{\partial E_y} \right) + \frac{1}{E} \frac{\partial^2 \tilde{g}}{\partial \xi^2} \right]. \quad (38)$$

In the first term, the velocity can be approximated by unity: $\langle v_z \rangle \approx 1$, i.e. the term $\partial \tilde{g} / \partial z (1 - \langle v_z \rangle)$ can be neglected. However the term $i\omega \tilde{g}(z; \xi, E_y) (1 - \langle v_z \rangle)$ has to be kept because of (37). Using the expression (33) for $\langle v_z \rangle$, one obtains from (38) the following partial differential equation for $\tilde{g}(z; \xi, E_y)$

$$\begin{aligned} \frac{\partial \tilde{g}(z; \xi, E_y)}{\partial z} + \frac{i\omega}{2\gamma^2} \tilde{g}(z; \xi, E_y) &= D_0 \frac{\partial}{\partial E_y} \left(E_y \frac{\partial \tilde{g}(z; \xi, E_y)}{\partial E_y} \right) \\ -i\omega \frac{E_y}{2E} \tilde{g}(z; \xi, E_y) + \frac{D_0}{E} \frac{\partial^2 \tilde{g}(z; \xi, E_y)}{\partial \xi^2} &- i\omega \frac{\xi^2}{2} \tilde{g}(z; \xi, E_y) \end{aligned} \quad (39)$$

This equation can be solved by the method of separation of variables. Putting $\tilde{g}(z; \xi, E_y) = \mathcal{Z}(z)\Xi(\xi)\mathcal{E}(E_y)$, after substitution into (39) we obtain a set of ordinary differential equations:

$$\frac{D_0}{E} \frac{1}{\Xi(\xi)} \frac{d^2\Xi(\xi)}{d\xi^2} - i\omega \frac{\xi^2}{2} = \mathcal{C}_\xi, \quad (40)$$

$$\frac{D_0}{\mathcal{E}(E_y)} \frac{d}{dE_y} \left(E_y \frac{d\mathcal{E}(E_y)}{dE_y} \right) - i\omega \frac{E_y}{2E} = \mathcal{C}_y, \quad (41)$$

$$\frac{1}{\mathcal{Z}(z)} \frac{d\mathcal{Z}(z)}{dz} + \frac{i\omega}{2\gamma^2} = \mathcal{C}_z, \quad (42)$$

where \mathcal{C}_z , \mathcal{C}_ξ and \mathcal{C}_y do not depend on any of the variables z , ξ and E_y and satisfy the condition

$$\mathcal{C}_z = \mathcal{C}_\xi + \mathcal{C}_y. \quad (43)$$

4.4. Solving the equation for $\Xi(\xi)$

Equation (40) can be rewritten as

$$\frac{d^2\Xi(\xi)}{d\xi^2} - i \frac{\omega E}{2D_0} \xi^2 \Xi(\xi) = \frac{E}{D_0} \mathcal{C}_\xi \Xi(\xi). \quad (44)$$

We change the variable

$$\chi = e^{i\pi/8} \sqrt[4]{\frac{\omega E}{2D_0}} \xi \quad (45)$$

and introduce the notation

$$\Omega = -e^{-i\pi/4} \sqrt{\frac{2E}{\omega D_0}} \mathcal{C}_\xi. \quad (46)$$

This results into

$$\frac{d^2\Xi(\chi)}{d\chi^2} - \chi^2 \Xi(\chi) = -\Omega \Xi(\chi). \quad (47)$$

This equation has the form of the Schrödinger equation for the harmonic oscillator. Its eigenvalues and integrable eigenfunctions are well known:

$$\Omega_n = 2n + 1 \quad (48)$$

$$\Xi_n(\chi) = H_n(\chi) \exp(-\chi^2/2), \quad (49)$$

where $n = 0, 1, 2, \dots$ and $H_n(\chi) = e^{\chi^2} \left(-\frac{d}{d\chi}\right)^n e^{-\chi^2}$ are Hermite Polynomials satisfying the orthogonality condition

$$\int_{-\infty}^{+\infty} d\chi e^{-\chi^2} H_n(\chi) H_{n'}(\chi) = \delta_{nn'} 2^n n! \sqrt{\pi} \quad (50)$$

which is equivalent to

$$\int_{-\infty}^{+\infty} d\chi \Xi_n(\chi) \Xi_{n'}(\chi) = \delta_{nn'} 2^n n! \sqrt{\pi}. \quad (51)$$

Returning back to the variable ξ one obtains

$$\Xi_n(\xi) = H_n \left(e^{i\pi/8} \sqrt[4]{\frac{\omega E}{2D_0}} \xi \right) \exp \left(-\frac{1+i}{4} \sqrt{\frac{\omega E}{D_0}} \xi^2 \right), \quad (52)$$

Any integrable function $F(\xi)$ can be represented as series

$$F(\xi) = F \left(e^{-i\pi/8} \sqrt[4]{\frac{2D_0}{\omega E}} \chi \right) = \sum_{n=0}^{\infty} \mathbf{b}_n \Xi_n(\chi) \quad (53)$$

Let us multiply the above expression by $\Xi_{n'}(\chi)$ and integrate over χ

$$\int_{-\infty}^{+\infty} d\chi F \left(e^{-i\pi/8} \sqrt[4]{\frac{2D_0}{\omega E}} \chi \right) \Xi_{n'}(\chi) = \sum_{n=0}^{\infty} \mathbf{b}_n \int_{-\infty}^{+\infty} d\chi \Xi_n(\xi) \Xi_{n'}(\xi) \quad (54)$$

Using (50) one finds

$$\mathbf{b}_n = \frac{1}{2^n n! \sqrt{\pi}} \int_{-\infty}^{+\infty} d\chi e^{-\chi^2/2} F \left(e^{-i\pi/8} \sqrt[4]{\frac{2D_0}{\omega E}} \chi \right) H_n(\chi) \quad (55)$$

From (46) and (48) one finds

$$\mathcal{C}_{\xi,n} = -(1+i) \sqrt{\frac{\omega D_0}{E}} \left(n + \frac{1}{2} \right), \quad n = 0, 1, 2, \dots \quad (56)$$

4.5. Solving the equation for $\mathcal{E}(E_y)$

Equation (41) can be rewritten as

$$\frac{d}{dE_y} \left(E_y \frac{d\mathcal{E}(E_y)}{dE_y} \right) - \left(\frac{i\omega}{2D_0E} E_y + \frac{C_y}{D_0} \right) \mathcal{E}(E_y) = 0, \quad (57)$$

By the substitution

$$E_y = \frac{1-i}{2} \sqrt{\frac{D_0E}{\omega}} \varepsilon \quad (58)$$

equation (57) can be reduced to

$$\varepsilon \frac{d^2\mathcal{E}}{d\varepsilon^2} + \frac{d\mathcal{E}}{d\varepsilon} - \left(\frac{\varepsilon}{4} - \frac{2\nu+1}{2} \right) \mathcal{E} = 0 \quad (59)$$

with

$$2\nu+1 = -(1-i) \sqrt{\frac{E}{\omega D_0}} C_y. \quad (60)$$

Further substitution $\mathcal{E}(\varepsilon) = \exp(-\varepsilon/2)L(\varepsilon)$ results into the Laguerre equation:

$$\varepsilon \frac{d^2L}{d\varepsilon^2} + (1-\varepsilon) \frac{dL}{d\varepsilon} + \nu L = 0 \quad (61)$$

One of two linearly independent solutions of this equation is logarithmically divergent at $\varepsilon \rightarrow 0$ and, therefore, has to be rejected. Another solution, $L_\nu(\varepsilon)$, is finite at $\varepsilon = 0$ and is known as the Laguerre function.²

Returning back to the variable E_y , the solution of equation (57) can be represented as

$$\mathcal{E}(E_y) = \exp\left(-\frac{1+i}{2} \sqrt{\frac{\omega}{D_0E}} E_y\right) L_\nu\left((1+i) \sqrt{\frac{\omega}{D_0E}} E_y\right) \quad (62)$$

The eigenvalues can be found by imposing the boundary conditions. If the energy of the channeling oscillations exceeds the value U_{\max} (see Fig. 2.1) the particle enters the region of high electron density, get scattered by crystal constituents and becomes dechanneled. Therefore, the distribution function

² At nonnegative integer values of ν , the Laguerre function is reduced to the well known Laguerre polynomials. In the general case that is relevant to our consideration, it can be represented by an infinite series (Appendix A.12).

of channeling particles has to be zero at $E_y = U_{\max}$. This results into the following boundary condition

$$L_\nu \left((1+i) \sqrt{\frac{\omega}{D_0 E}} U_{\max} \right) = 0. \quad (63)$$

Equation (63) has to be solved for ν . Then, according to (60), the eigenvalue $\mathcal{C}_{y,k}$ can be found from

$$\mathcal{C}_y = -\frac{(1+i)}{2} \sqrt{\frac{D_0 \omega}{E}} (2\nu + 1). \quad (64)$$

The subscript $k = 1, 2, 3, \dots$ enumerates different roots of equation (63).

We introduce a dimensionless parameter

$$\kappa = \frac{4}{j_{0,1}^2} \frac{\omega}{D_0 E} U_{\max}^2 \quad (65)$$

($j_{0,k}$ is k -th zero of the 0-th order Bessel function: $J_0(j_{0,k}) = 0$). Then equation (63) can be rewritten as

$$L_\nu \left(\frac{1+i}{2} j_{0,1} \sqrt{\kappa} \right) = 0. \quad (66)$$

This equation has infinite number of complex roots (see Appendix) which we denote as $\nu_k(\kappa)$, $k = 1, 2, 3, \dots$. The equation does not have any analytical solution and therefore has to be solved numerically.

Instead of the complex function $\nu_k(\kappa)$, it is more convenient to introduce two real functions:

$$\alpha_k(\kappa) = \frac{\sqrt{\kappa}}{j_{0,1}} [1 + 2 (\Re[\nu_k(\kappa)] - \Im[\nu_k(\kappa)])] \quad (67)$$

$$\beta_k(\kappa) = \frac{1}{2j_{0,1}\sqrt{\kappa}} [1 + 2 (\Re[\nu_k(\kappa)] + \Im[\nu_k(\kappa)])]. \quad (68)$$

The eigenvalues (64) can be represented in the form

$$\mathcal{C}_{y,k} = -\frac{\alpha_k(\kappa)}{L_d} - i\omega\theta_L^2\beta_k(\kappa). \quad (69)$$

Here

$$L_d = 4U_{\max}/(j_{0,1}^2 D_0) \quad \text{and} \quad (70)$$

$$\theta_L = \sqrt{2U_{\max}/E} \quad (71)$$

are, respectively, the dechanneling length [32] and Lindhard's angle. The parameter κ (65) can be rewritten in terms of L_d and θ_L

$$\kappa = \pi \frac{L_d}{\lambda} \theta_L^2, \quad (72)$$

where $\lambda = 2\pi/\omega$ is the spatial period of the modulation.

4.6. Solving the equation for $\mathcal{Z}(z)$

Equation (42) has the solution

$$\mathcal{Z}(z) = \exp \left(\mathcal{C}_z - i \frac{\omega}{2\gamma^2} z \right) \quad (73)$$

The value of \mathcal{C}_z can be found using (43), (56) and (64). Then the solution (73) takes the form

$$\begin{aligned} \mathcal{Z}_{n,k}(z) = & \exp \left\{ -\frac{z}{L_d} \left[\alpha_k(\kappa) + (2n+1) \frac{\sqrt{\kappa}}{j_{0,1}} \right] - \right. \\ & \left. i\omega z \left[\frac{1}{2\gamma^2} + \theta_L^2 \beta_k(\kappa) + \theta_L^2 \frac{(2n+1)}{2j_{0,1}\sqrt{\kappa}} \right] \right\}. \end{aligned} \quad (74)$$

Hence, the solution of Eq. (35) is represented as

$$g(z; \xi, E_y) = \exp(-i\omega z) \sum_{n=0}^{\infty} \sum_{k=1}^{\infty} \mathbf{a}_{n,k} \Xi_n(\xi) \mathcal{E}_k(E_y) \mathcal{Z}_{n,k}(z), \quad (75)$$

where the coefficients $\mathbf{a}_{n,k}$ are found from the particle distribution at the entrance of the crystal channel:

$$\mathbf{a}_{n,k} = \frac{\int_{-\infty}^{+\infty} d\xi \int_0^{U_{\max}} dE_y g(0; \xi, E_y) \Xi_n(\xi) \mathcal{E}_k(E_y)}{2^n n! \sqrt{\pi} \int_0^{U_{\max}} dE_y [\mathcal{E}_k(E_y)]^2}. \quad (76)$$

5. The demodulation length

5.1. The demodulation length in a straight channel

Due to the exponential decrease of $\mathcal{Z}_{n,k}(z)$ with z (see (74)), the asymptotic behaviour of $\tilde{g}(z; \xi, E_y)$ at large z is dominated by the term with $n = 0$ and $k = 1$ having the smallest value of the factor $[\alpha_k(\kappa) + (2n+1)\sqrt{\kappa}/j_{0,1}]$

in the exponential. Therefore, at sufficiently large penetration depths, the particle distribution depends on z as

$$g(z; \xi, E_y) \propto \exp(-z/L_{\text{dm}} - i\omega/u_z z) \quad (77)$$

where L_{dm} is the newly introduced parameter — *the demodulation length*:

$$L_{\text{dm}} = \frac{L_{\text{d}}}{\alpha_1(\kappa) + \sqrt{\kappa}/j_{0,1}} \quad (78)$$

and u_z is the phase velocity of the modulated beam along the crystal channel

$$u_z = \left[1 + \frac{1}{2\gamma^2} + \theta_{\text{L}}^2 \left(\beta_k(\kappa) + \frac{1}{2j_{0,1}\sqrt{\kappa}} \right) \right]^{-1}. \quad (79)$$

This parameter is important for establishing the resonance conditions between the undulator parameters and the radiation wavelength.

In this article we concentrate our attention on the demodulation length. This parameter represents the characteristic scale of the penetration depth at which a beam of channeling particles loses its modulation.

Fig. 5.1 presents the dependence of the ratio $L_{\text{dm}}/L_{\text{d}}$ on the parameter κ . It is seen that the demodulation length approaches the dechanneling length at $\kappa \lesssim 1$. On the contrary, the ratio noticeably drops for $\kappa \gtrsim 10$.

It is instructive to study the influence of the particle motion in x and y direction on the demodulation length separately. Replacing $\alpha_1(\kappa)$ in (78) with unity means neglecting the motion in the y direction, while omitting the second term in the denominator ignores the motion in x direction. One sees from Fig. 5.1 that it is mostly the motion in x direction that diminishes the demodulation length at $\kappa \lesssim 10$, while the influence of channeling oscillations is negligible. This suggests the idea that for the axial channeling, i.e. when motion in both x and y directions has the nature of channeling oscillations, the demodulation length L_{dm} may practically coincide with the dechanneling length L_{d} at higher frequencies of the beam modulation than in the case of planar channeling.

5.2. The centrifugal force in a bent channel

So far, beam demodulation in a straight channel has been considered. The channels of a crystalline undulator, however, have to be periodically bent. Therefore the above formalism has to be modified for the case of a bent channel.

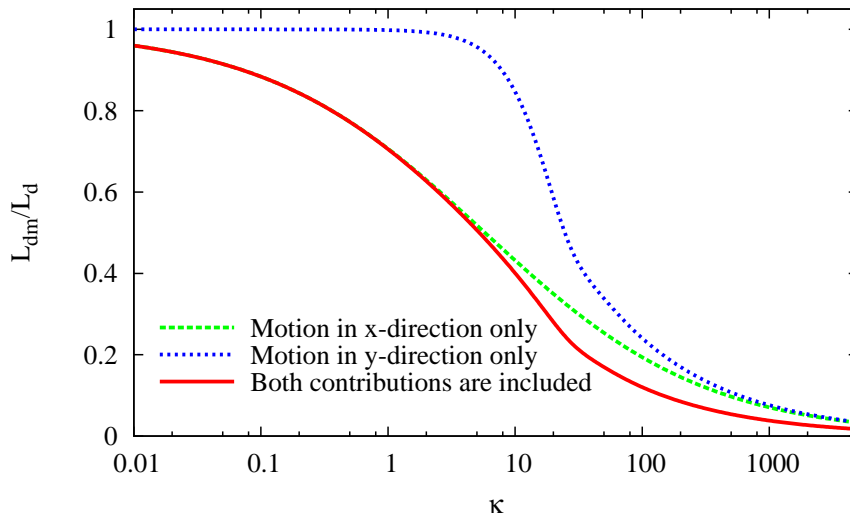


Figure 5: The ratio of the demodulation length L_{dm} (78) to the dechanneling length L_{d} versus the parameter κ (72). See text for details.

Let us consider a crystal that is bent in the (yz) plane so that the crystal channel has a constant curvature with the radius R . An ultrarelativistic particle with energy E moving in such a channel experiences the action the centrifugal force

$$F_{\text{c.f.}} = \frac{E}{R}. \quad (80)$$

It is convenient to characterise the channel curvature by the dimensionless parameter C defined as

$$C = \left| \frac{F_{\text{c.f.}}}{U'_{\text{max}}} \right|, \quad (81)$$

where U'_{max} is the maximum value of the derivative of the particle potential energy in the channel, i.e. the maximum transverse force acting on the particle in the interplanar potential. Channeling is possible at $0 \leq C < 1$. The value $C = 0$ corresponds to a straight channel. The critical radius R_c (known also as Tsyganov radius) at which the interplanar potential becomes unable to overcome the centrifugal force corresponds to $C = 1$.

In the case of potential energy (1),

$$U'_{\text{max}} = U'(\rho_{\text{max}}) = 2 \frac{U_{\text{max}}}{\rho_{\text{max}}}. \quad (82)$$

so that

$$C = \frac{\rho_{\max} F_{\text{c.f.}}}{2U_{\max}}. \quad (83)$$

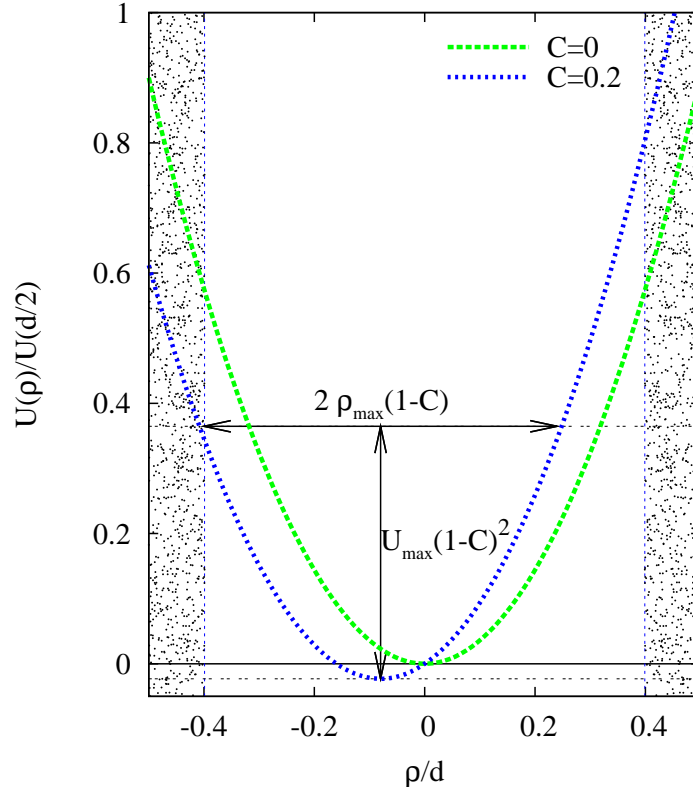


Figure 6: The potential energy of a particle in the planar crystal channel for a straight, $C = 0$, and for a bent, $C \neq 0$, crystal. The effective width of the bent channel is $2\rho_{\max}(1-C)$ and the depth of the potential well is $U_{\max}(1-C)^2$, where $2\rho_{\max}$ and U_{\max} are, respectively, the effective width and the depth of the straight channel (cf. Fig. 2.1).

The potential energy is modified by the centrifugal force in the following way

$$U_C(\rho) = U(\rho) - \rho F_{\text{c.f.}}. \quad (84)$$

For the parabolic potential energy (1) the modified potential can be conve-

niently rewritten in terms of the parameter C :

$$U_C(\rho) = U_{\max} \left[\left(\frac{\rho}{\rho_{\max}} - C \right)^2 - C^2 \right] \quad (85)$$

The potential energy $U_C(\rho)$ reaches its minimum at $\rho_0 = C\rho_{\max}$. The effective width of the channel becomes (see Fig. 5.2)

$$\rho_{\max} - \rho_0 = \rho_{\max}(1 - C). \quad (86)$$

The depth of the potential energy well is

$$U_C(\rho_{\max}) - U_C(\rho_0) = U_{\max}(1 - C)^2. \quad (87)$$

So to obtain the solution of the diffusion equation for the bent crystal we can use the results of Sec. 4 with the substitution

$$U_{\max} \rightarrow U_{\max}(1 - C)^2. \quad (88)$$

5.3. The demodulation length in a bent channel

Substitution (88) modifies the demodulation length and the Lindhard's angle the parameter κ in the following way:

$$L_d \rightarrow L_d(1 - C)^2 \quad (89)$$

$$\theta_L \rightarrow \theta_L(1 - C) \quad (90)$$

Consequently, the the modification of parameter κ is

$$\kappa \rightarrow \kappa(1 - C)^4. \quad (91)$$

It is convenient to introduce modified functions $\alpha_k(\kappa, C)$ and $\beta_k(\kappa, C)$:

$$\alpha_k(\kappa, C) = \frac{\alpha_k(\kappa(1 - C)^4)}{(1 - C)^2} \quad (92)$$

$$\beta_k(\kappa, C) = (1 - C)^2 \beta_k(\kappa(1 - C)^4). \quad (93)$$

In terms of these functions, the eigenvalue $\mathcal{C}_{y,k}$ has the form

$$\mathcal{C}_{y,k} = -\frac{\alpha_k(\kappa, C)}{L_d} - i\omega\theta_L^2\beta_k(\kappa, C). \quad (94)$$

This exactly coincides with (69) up to replacing $\alpha_k(\kappa)$ and $\beta_k(\kappa)$ with $\alpha_k(\kappa, C)$ and $\beta_k(\kappa, C)$, respectively. Note that L_d and θ_L in (94) have the same meaning as in (69): they are related to the straight channel.

Similarly, the demodulation length in the bent channel is given by

$$L_{\text{dm}} = \frac{L_d}{\alpha_1(\kappa, C) + \sqrt{\kappa}/j_{0,1}} \quad (95)$$

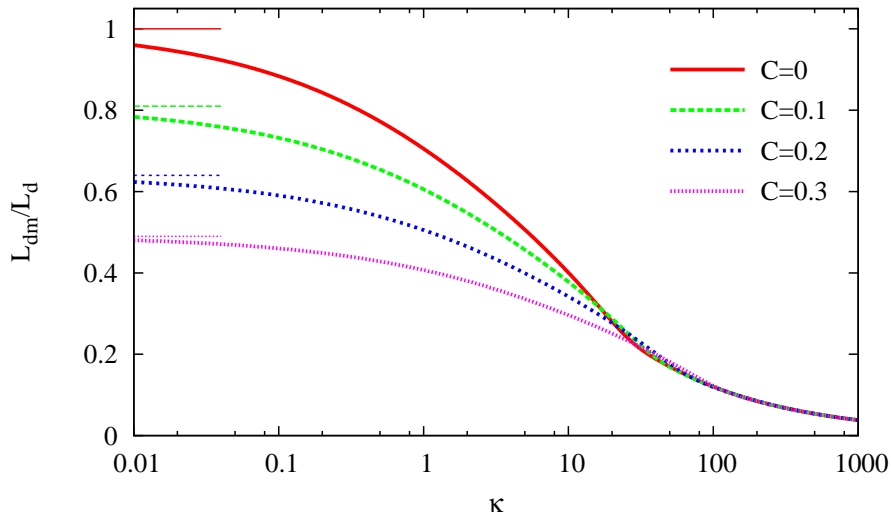


Figure 7: The ratio of the demodulation length L_{dm} (95) to the dechannelling length in the straight channel L_d versus the parameter κ (72) for different values of curvature parameter C . The corresponding asymptotic values at $\kappa \rightarrow 0$ are shown by thin horizontal lines.

Fig. 5.1 presents the dependence of the ratio L_{dm}/L_d on the parameter κ . At $\kappa \rightarrow 0$, the demodulation length approaches $(1 - C)^2 L_d$ which is the dechannelling length in a bent crystal. It is seen that the demodulation length is smaller than dechannelling length by only 20–30% at $\kappa \lesssim 1$ for C ranging from 0 to 0.3. It noticeably drops, however, at $\kappa \gtrsim 10$.

The above estimations are made for the channel with constant curvature. Similar results are expected for a sinusoidal channel with C varying between 0 and 0.3.

It was proven for a number crystals channels [18] that the dechannelling length of positrons is sufficiently large to make the crystalline undulator

feasible. Such a crystalline undulator becomes a CUL, i.e. it generates coherent radiation, provided that it is fed by a modulated positron beam and the beam preserves its modulation over the length of the crystal. This takes place if the demodulation length in the crystalline undulator is not much smaller than the dechannelling length. Hence, CUL is feasible if there exist crystal channels ensuring $\kappa \lesssim 1$ in the range of the photon energies above ~ 100 keV (softer photons are strongly absorbed in the crystal). It will be shown in the next section that such crystal channels do exist.

5.4. Estimation of the parameter κ

To evaluate the parameter κ (72) we shall use the approximate formula for the dechannelling length [32]:

$$L_d = \frac{256}{9\pi^2} \frac{E}{m_e} \frac{a_{\text{TF}}}{r_0} \frac{d}{\Lambda}. \quad (96)$$

Here m_e and r_0 are, respectively, the electron mass and the classical radius, d is the distance between the crystal planes, and the Coulomb logarithm Λ for positron projectiles is defined as [18]:

$$\Lambda = \log \frac{\sqrt{2Em_e}}{I} - \frac{23}{24}, \quad (97)$$

with

$$I \approx 16Z^{0.9} \text{ eV} \quad (98)$$

being the ionization potential of the crystal atom with the atomic number Z . The Thomas-Fermi radius of this atom is related to the Bohr radius a_B by the formula

$$a_{\text{TF}} = a_B \frac{0.8853}{\sqrt[3]{Z}}. \quad (99)$$

Substituting (96) into (72) and taking into account (71), one obtains

$$\kappa = \frac{512}{9\pi} \frac{a_{\text{TF}}}{\Lambda r_0} \frac{U_{\text{max}}}{m_e} \frac{d}{\lambda}. \quad (100)$$

As is seen from the above formula the value of κ is determined by the potential depth U_{max} , by the distance between the planes d and the modulation period λ . It also depends on the atomic number of the crystal atoms Z via (98) and (99). These parameters are listed in table 5.4 for several crystal channels.

Table 1: The parameters of the crystalchannels used in the calculations (see text). For (111) plane of diamond, only the larger of two channels is presented.

Crystal	Z	I (eV)	a_{TF} (Å)	Plane	d (Å)	U_{max} (eV)
Diamond	6	80	0.26	(100)	0.9	2.2
				(110)	1.3	7.3
				(111)L	1.5	10.8
Graphite	6	80	0.26	(0002)	3.4	37.9
Silicon	14	172	0.19	(100)	1.4	6.6
				(110)	1.9	13.5
Germanium	32	362	0.15	(100)	1.4	14.9
Tungsten	74	770	0.11	(100)	1.6	56.3

The dependence on the particle energy is cancelled out, except the weak dependence due to the logarithmic expression (97).

The dependence of the parameter κ on the energy of the emitted photons, $\hbar\omega = 2\pi\hbar/\lambda$, is shown in Fig. 5.4. The calculation was done for 1 GeV positrons. Due to the weak (logarithmic) dependence of κ on the particle energy, changing this energy by an order of magnitude would leave Fig. 5.4 practically unaltered.

As one sees from the figure, $\kappa \sim 1$ corresponds to $\hbar\omega = 100 - 300$ keV for (100) and (110) planes in Diamond and (100) plane in Silicon. So these channels are the most suitable candidates for using in CUL. This is, however, not the case for a number of other crystals e.g. for graphite and tungsten having $\kappa \gtrsim 10$ in the same photon energy range.

At $\hbar\omega \sim 10$ MeV, κ becomes larger than 10 for all crystal channels. This puts the upper limit on the energies of the photons that can be generated by CUL. It is expected to be most successful in the hundred keV range, while generating MeV photons looks more challenging.

6. Discussion and Conclusion

One may expect that the demodulation is not limited to the processes illustrated in figure 3. An additional contribution can come from the energy spread of the channelling particles, as it usually happens in ordinary FELs. In fact, the contribution of the energy spread to the beam demodulation

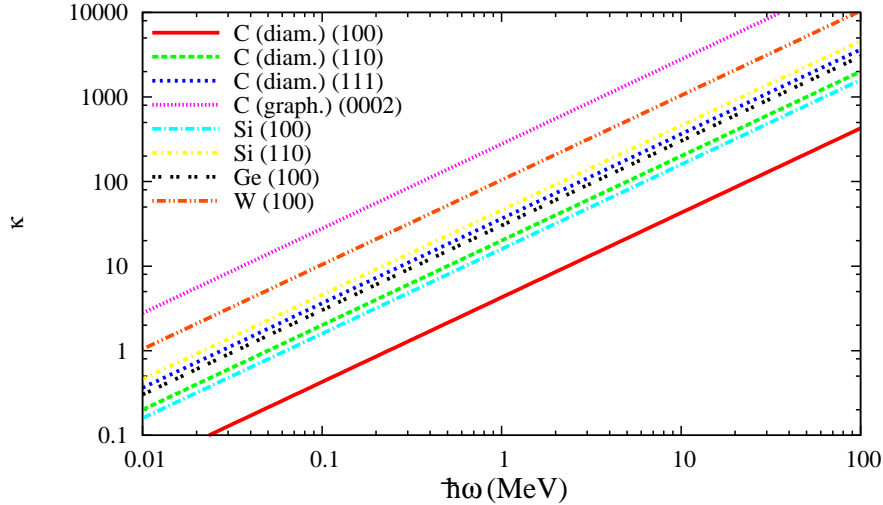


Figure 8: The parameter κ (72) versus the photon energy $\hbar\omega$ for the crystal channels listed in Table 5.4.

on the distance of a few dechannelling lengths is negligible. It would be substantial if the relative *spread* $\delta E/E$ of particle energies would be comparable to or larger than the ratio λ_u/L_d . The latter ratio, however, can not be made smaller than 10^{-2} [18],³ while modern accelerators usually have a much smaller relative energy spread. The same is true for the energy spread induced by the stochastic energy losses of the channelling particles due to the interaction with the crystal constituents and the radiation of photon. It was shown in Ref.[33] that at initial energies of $\sim 1\text{GeV}$ or smaller, the average relative energy *losses* of a positron in the crystalline undulator $\Delta E/E$ are smaller than 10^{-2} . Clearly, the induced energy *spread* $\delta E/E \ll \Delta E/E$ is safely below the ratio λ_u/L_d . From these reasons, we ignored energy spread of the particles in our calculations.

In conclusion, we have studied the propagation of a modulated positron beam in straight and bent planar crystal channel within the diffusion ap-

³Note that the corresponding quantity in ordinary ultraviolet and soft x-ray FELs, the inverse number of undulator periods $1/N_u = \lambda_u/L$, is usually of the order of 10^{-3} – 10^{-4} [31]. That is why these FELs are so demanding to the small energy spread of the electron beam.

proach and presented a detailed description of the used formalism. We introduced a new parameter, the demodulation length, which characterizes the penetration depth at which the beam preserves its modulation. It has been demonstrated that one can find the crystal channels where the demodulation length sufficient for producing coherent radiation with the photon energy of hundreds of keV. This opens the prospects for creating intense monochromatic radiation sources in a frequency range which is unattainable for conventional free electron lasers. Developing suitable methods of beam modulation would be the next milestone on the way towards this goal.

Appendix A. Appendix: Solving equation (66).

Appendix A.1. A series expansion at $\kappa \ll 1$

At small values of κ , the solution of equation (66) can be found in the form of power series.

The Laguerre function $L_\nu(\mathfrak{z})$ (which is a special case of the Kummer function, $L_\nu(\mathfrak{z}) \equiv M(-\nu, 1, \mathfrak{z})$) can be represented as

$$L_\nu(\mathfrak{z}) = \exp(\mathfrak{z}/2) \sum_{n=0}^{\infty} A_n \left[\frac{\mathfrak{z}}{2(1+2\nu)} \right]^{n/2} J_n \left(\sqrt{2(1+2\nu)\mathfrak{z}} \right), \quad (\text{Appendix A.1})$$

where $J_n(\dots)$ are Bessel functions and the coefficients A_n are defined by the following recurrence relation:

$$A_0 = 1 \quad (\text{Appendix A.2})$$

$$A_1 = 0 \quad (\text{Appendix A.3})$$

$$A_2 = \frac{1}{2} \quad (\text{Appendix A.4})$$

$$A_{n+1} = \frac{1}{n+1} [nA_{n-1} - (1+2\nu)A_{n-2}]. \quad (\text{Appendix A.5})$$

Keeping only the leading term in (Appendix A.1) (this approximation is valid if $\mathfrak{z} \ll 1$), equation (66) can be reduced to

$$J_0 \left(\sqrt{(1+2\nu^{(0)})(1+i)j_{0,1}\sqrt{\kappa}} \right) = 0, \quad (\text{Appendix A.6})$$

where $\nu^{(0)}$ is the zero-order approximation to the root of equation (66).

Equation (Appendix A.6) is satisfied if

$$\sqrt{(1 + 2\nu_k^{(0)})(1 + i)j_{0,1}\sqrt{\kappa}} = j_{0,k}, \quad (\text{Appendix A.7})$$

$j_{0,k}$ is a root of the Bessel function: $J_0(j_{0,k}) = 0$. Here the subscript $k = 1, 2, 3, \dots$ enumerates the roots of the Bessel function and the corresponding approximate solutions of equation (66). Solving (Appendix A.7) for $\nu_k^{(0)}$ results into

$$\nu_k^{(0)}(\kappa) = \frac{1 - i j_{0,k}^2}{4} \frac{1}{j_{0,1} \sqrt{\kappa}} - \frac{1}{2}. \quad (\text{Appendix A.8})$$

Keeping higher order terms in (Appendix A.1) and expanding the Bessel functions around the the zero-order approximation (Appendix A.8), one obtains a series expansion of $\nu_k(\kappa)$:

$$\begin{aligned} \nu_k(\kappa) = & \frac{1 - i j_{0,k}^2}{4} \frac{1}{j_{0,1} \sqrt{\kappa}} - \frac{1}{2} + \frac{1 + i}{24} j_{0,1} \frac{j_{0,k}^2 - 2}{j_{0,k}^2} \sqrt{\kappa} \\ & - \frac{1 - i}{720} j_{0,1}^3 \frac{j_{0,k}^4 - 17j_{0,k}^2 + 54}{j_{0,k}^6} (\sqrt{\kappa})^3 + (\text{Appendix A.9}) \end{aligned}$$

(Dots stand for higher order terms with respect to κ). For the functions (67) and (68) expansion (Appendix A.9) takes the form

$$\alpha_k(\kappa) = \frac{j_{0,k}^2}{j_{0,1}^2} - \frac{j_{0,1}^2 (j_{0,k}^4 - 17j_{0,k}^2 + 54)}{180j_{0,k}^6} \kappa^2 + (\text{Appendix A.10})$$

$$\beta_k(\kappa) = \frac{j_{0,k}^2 - 2}{12j_{0,k}^2} + \dots \quad (\text{Appendix A.11})$$

Appendix A.2. Numerical solution

Expansions (Appendix A.9), (Appendix A.10) and (Appendix A.11) fail at $\kappa \gtrsim 1$. Therefore, equation (66) has to be solved numerically. In our numerical procedure, we use the series representation for $L_\nu(\mathfrak{z})$:

$$L_\nu(\mathfrak{z}) = \sum_{j=0}^{\infty} \frac{\prod_{m=0}^{j-1} (m - \nu)}{(j!)^2} \mathfrak{z}^j \quad (\text{Appendix A.12})$$

Equation was solved by Newton's method. At small κ the value found from the series expansion (Appendix A.9) was used as initial approximation. Then κ was gradually increasing. At each step, the equation was

solved and the solution was used as initial approximation for the next step. During this procedure, the roots $\nu_k(\kappa)$ were slowly moving in the complex plane along the trajectories shown in figure Appendix A.2. The functions

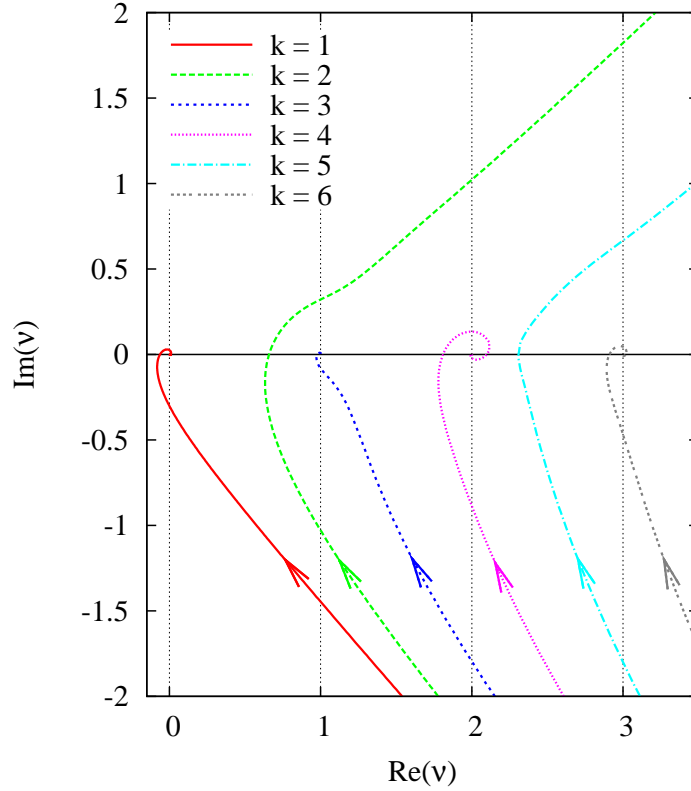


Figure A.9: The trajectories drawn by the roots $\nu_k(\kappa)$ of (66) in the complex plain at varying κ . The arrows show the direction of motion of the roots when κ increases.

α_k and β_k are plotted in Figures Appendix A.2 and Appendix A.2.

Appendix A.3. Asymptotic behaviour at $\kappa \gg 1$

As it is seen from Figure Appendix A.2, some of $\nu_k(\kappa)$ approaches integer real numbers as $\kappa \rightarrow \infty$. This the case for $k = 1, 3, 4, 6$. For these solutions, the asymptotic behaviour can be found.

Let us represent $\nu_k(\kappa)$ in the form

$$\nu_k(\kappa) = n_k + \delta_k(\kappa), \quad (\text{Appendix A.13})$$

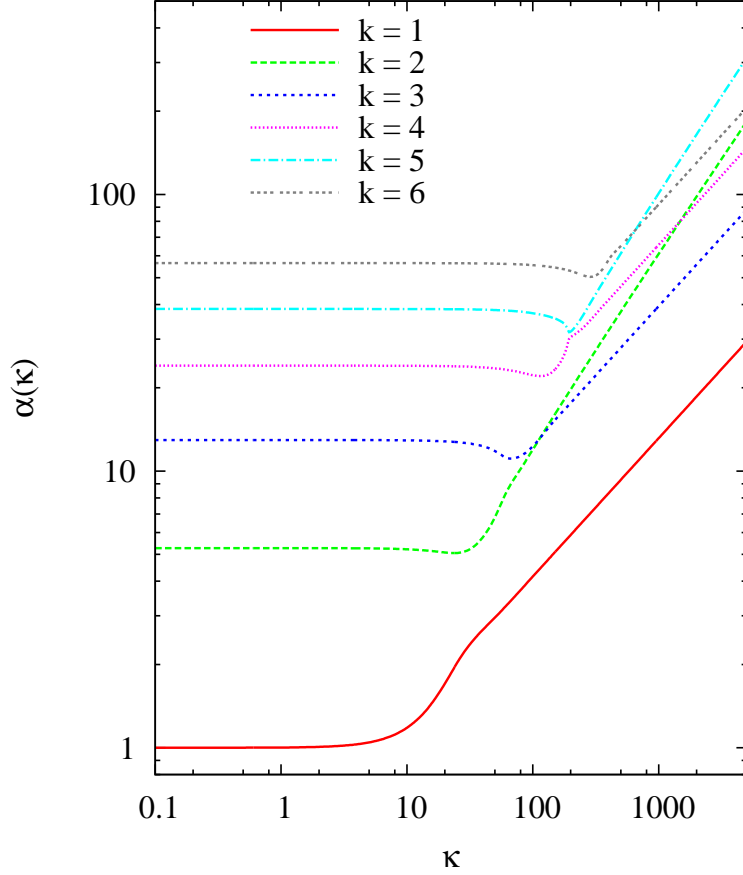


Figure A.10: The function $\alpha_k(\kappa)$ obtained by numerical analysis.

where $n_k = \nu_k(\infty)$ is an integer number and the function $\delta_k(\kappa)$ goes to zero at $\kappa \rightarrow \infty$.

Substituting (Appendix A.13) into (Appendix A.12) and expanding around $\delta_k = 0$ one obtains

$$\begin{aligned}
 L_\nu(\mathfrak{z}) = & n_k! \left[\sum_{j=0}^{n_k} \frac{(-1)^j}{(j!)^2 [n_k - j]!} \mathfrak{z}^j \right. & (\text{Appendix A.14}) \\
 & \left. - \delta_k \left(P_{n_k}(\mathfrak{z}) + (-1)^{n_k} \mathfrak{z}^{n_k+1} \sum_{j=0}^{\infty} \frac{j!}{[(j + n_k + 1)!]^2} \mathfrak{z}^j \right) \right]
 \end{aligned}$$

Here $P_{n_k}(\mathfrak{z})$ is a polynomial of the order n_k whose explicit form will not be

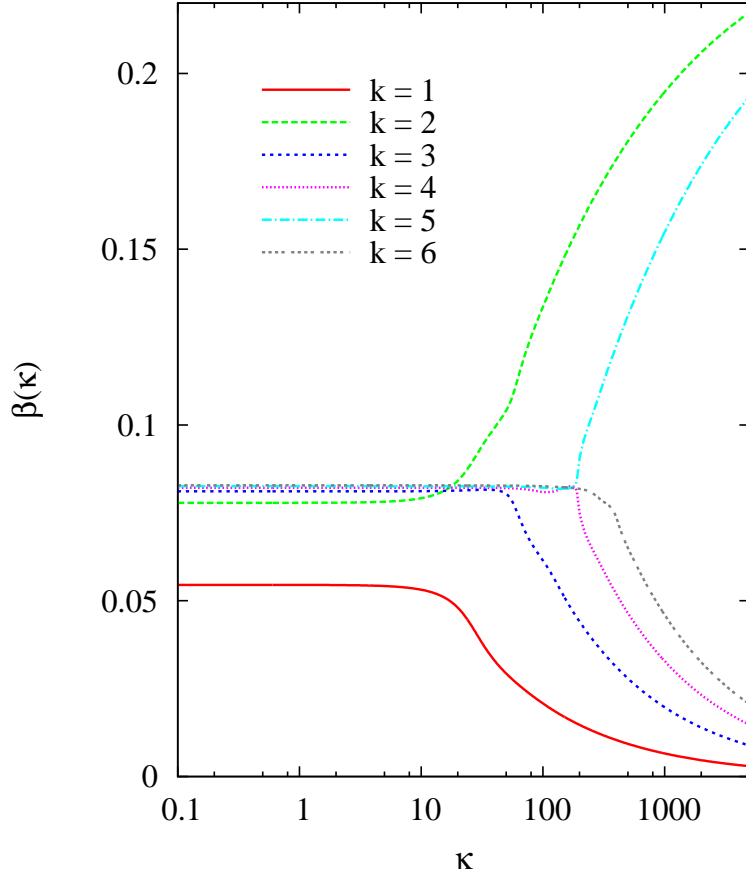


Figure A.11: The function $\beta_k(\kappa)$ obtained by numerical analysis.

needed in the following.

At $|\mathfrak{z}| \ll 1$, the infinite sum in (Appendix A.14) can be approximated by an integral and evaluated by Laplace's method:

$$\sum_{j=0}^{\infty} \frac{j!}{[(j + n_k + 1)!]^2} \mathfrak{z}^j \simeq \mathfrak{z}^{-2(n_k+1)} e^{\mathfrak{z}} \quad (\text{Appendix A.15})$$

The polynomial $P_{n_k}(\mathfrak{z})$ in (Appendix A.14) becomes negligible with respect to the exponential at large \mathfrak{z} . Similarly, the leading order term dominates the first sum in (Appendix A.14). The asymptotic expression for $L_\nu(\mathfrak{z})$ takes,

therefore, the following form

$$L_\nu(\mathfrak{z}) \asymp (-1)^{n_k} n_k! \left[\frac{\mathfrak{z}^{n_k}}{(n_k!)^2} - \delta_k \mathfrak{z}^{-(n_k+1)} e^{\mathfrak{z}} \right] \quad (\text{Appendix A.16})$$

Using (Appendix A.16) and taking into account (Appendix A.13) one obtains the asymptotic expression for the root of equation (66):

$$\nu_k(\kappa) \asymp n_k + \frac{1}{(n_k!)^2} \left(\frac{1+i}{2} j_{0,1} \sqrt{\kappa} \right)^{2n_k+1} \exp \left(-\frac{1+i}{2} j_{0,1} \sqrt{\kappa} \right). \quad (\text{Appendix A.17})$$

This equivalent to the following asymptotic behaviour of the functions (67) and (68)

$$\alpha_k(\kappa) \asymp \frac{2n_k+1}{j_{0,1}} \sqrt{\kappa} + \frac{(j_{0,1})^{2n_k} \kappa^{n_k+1}}{2^{n_k-1} (n_k!)^2} \exp \left(-\frac{j_{0,1} \sqrt{\kappa}}{2} \right) \sin \left(\frac{j_{0,1} \sqrt{\kappa}}{2} - \frac{\pi}{2} n_k \right) \quad (\text{Appendix A.18})$$

$$\beta_k(\kappa) \asymp \frac{2n_k+1}{2j_{0,1} \sqrt{\kappa}} + \frac{(j_{0,1})^{2n_k} \kappa^{n_k}}{2^{n_k} (n_k!)^2} \exp \left(-\frac{j_{0,1} \sqrt{\kappa}}{2} \right) \cos \left(\frac{j_{0,1} \sqrt{\kappa}}{2} - \frac{\pi}{2} n_k \right) \quad (\text{Appendix A.19})$$

It has to be stressed once more, that not all solutions of equation (66) have the above asymptotic behaviour. Among the solutions represented in figures Appendix A.2-Appendix A.2, (Appendix A.17)–(Appendix A.19) is valid only for $k = 1, 3, 4, 6$ with $n_k = 0, 1, 2, 3$, respectively.

Acknowledgement

This work has been supported in part by the European Commission (the PECU project, Contract No. 4916 (NEST)) and by Deutsche Forschungsgemeinschaft.

References

- [1] A. Kostyuk, A.V. Korol, A.V. Solov'yov and W. Greiner, J. Phys. B: At. Mol. Opt. Phys. **43** 151001 (2010).
- [2] A. Kostyuk, A.V. Korol, A.V. Solov'yov and W. Greiner, "Modulated positron beam in a crystal channel", in "Charged and Neutral Particles Channeling Phenomena - Channeling 2008", Proceedings of the 51st Workshop of the INFN Eloisatron Project, Erice, Italy, 25 October – 1 November 2008, S.B. Dabagov and L. Palumbo, Eds., World Scientific, 2010.
- [3] A.V. Korol, A. V. Solov'yov and W. Greiner, J. Phys. G24 (1998), L45–53.
- [4] A.V. Korol, A. V. Solov'yov and W. Greiner, Int. J. Mod. Phys. E8 (1999) 49–100.
- [5] A. Kostyuk, A.V. Korol, A. V. Solov'yov, and W. Greiner, J. Phys. G36 (2009) 025107.
- [6] J. Lindhard, Kong. Danske Vid. Selsk. Mat.-Fys. Medd. 34 (1965) No. 14.
- [7] E.N. Tsyganov, TM-682, TM-684, Fermilab, Batavia (1976).
- [8] A.F. Elishev *et al.*, Phys. Lett. B88 (1979) 387.
- [9] A.G. Afonin *et al.*, Nucl. Instrum. Meth. B234 (2005) 14.
- [10] G. Arduini *et al.*, Phys. Lett. B422 (1998) 325.
- [11] W. Scandale *et al.*, Phys. Rev. ST Accel. Beams 11 (2008) 063501.
- [12] R.A. Carrigan *et al.*, Phys. Rev. ST Accel. Beams 5 (2002) 043501.
- [13] R.P. Flliller *et al.*, Phys. Rev. ST Accel. Beams 9 (2006) 013501.
- [14] S. Strokov *et al.*, J. Phys. Soc. Jap. 76 (2007) 064007.
- [15] E. Uggerhøj and U.I. Uggerhøj, Nucl. Instrum. Meth. B234 (2005) 31.
- [16] S. Bellucci *et al.*, Nucl. Instrum. Meth. B252 (2006) 3.

- [17] S. Strokov *et al.*, Nucl. Instrum. Meth. B252 (2006) 16.
- [18] A.V. Korol, A. V. Solov'yov and W. Greiner, Int. J. Mod. Phys. E13 (2004) 867–916.
- [19] M. Tabrizi, A.V. Korol, A. V. Solov'yov and W. Greiner, Phys. Rev. Lett. 98 (2007) 164801.
- [20] S. Bellucci *et al.*, Phys. Rev. Lett. 90 (2003) 034801.
- [21] V. Guidi *et al.*, Nucl. Inst. and Meth. B234, (2005) 40.
- [22] P. Balling *et al.*, Nucl. Inst. and Meth. B267 (2009) 2952.
- [23] M. B. H. Breese, Nucl. Inst. and Meth. B132 (1997) 540.
- [24] U. Mikkelsen and E. Uggerhøj, Nucl. Inst. and Meth. B160 (2000) 435.
- [25] A.V. Korol, W. Krause, A. V. Solov'yov, and W. Greiner Nucl. Inst. and Meth. A483 (2002) 455.
- [26] V. T. Baranov *et al.*, Nucl. Instrum. Meth. B252 (2006) 32.
- [27] H. Backe, P. Kunz, W. Lauth and A. Rueda, Nucl. Instrum. Meth. B266 (2008) 3835.
- [28] A.V. Korol, A. V. Solov'yov and W. Greiner, in: W. Greiner, J. Reinhardt (Eds.), Topics in Heavy Ion Physics - Proceedings of the Memorial Symposium for Gerhard Soff, Frankfurt am Main, Germany, April 25-28, EP Systema, Budapest, 2005, pp. 73–86.
- [29] V. L. Ginzburg, Izv. Akad. Nauk. SSSR, Ser. Fiz. 11 (1947) 165–182.
- [30] J. M. J. Madey, J. Appl. Phys. 42 (1971) 1906–1913.
- [31] P. Schmüser, M. Dohlus, J. Rossbach, Ultraviolet and Soft X-Ray Free-Electron Lasers, Springer, Berlin Heidelberg, 2008.
- [32] V. M. Biruykov, Yu. A. Chesnokov, V. I. Kotov, Crystal Channelling and its Application at High-Energy Accelerators, Springer, Berlin Heidelberg New York, 1996.
- [33] A.V. Korol, A. V. Solov'yov and W. Greiner, Int. J. Mod. Phys. E9 (2000) 77.